Gradual centriole maturation associates with the mitotic surveillance pathway in mouse development

Cally Xiao[1,2,3,4,†,‡] iD, Marta Grzonka[1,2,4,†], Charlotte Meyer-Gerards[1,2,4], Miriam Mack[1,2,5], Rebecca Figge[4] & Hisham Bazzi[1,2,*] iD

Abstract

Centrosomes, composed of two centrioles and pericentriolar material, organize mitotic spindles during cell division and template cilia during interphase. The first few divisions during mouse development occur without centrioles, which form around embryonic day (E) 3. However, disruption of centriole biogenesis in *Sas-4* null mice leads to embryonic arrest around E9. Centriole loss in *Sas-4$^{-/-}$* embryos causes prolonged mitosis and p53-dependent cell death. Studies *in vitro* discovered a similar USP28-, 53BP1-, and p53-dependent mitotic surveillance pathway that leads to cell cycle arrest. In this study, we show that an analogous pathway is conserved *in vivo* where 53BP1 and USP28 are upstream of p53 in *Sas-4$^{-/-}$* embryos. The data indicate that the pathway is established around E7 of development, four days after the centrioles appear. Our data suggest that the newly formed centrioles gradually mature to participate in mitosis and cilia formation around the beginning of gastrulation, coinciding with the activation of mitotic surveillance pathway upon centriole loss.

Introduction

Centrosomes are major microtubule organizing centers (MTOCs) of animal cells and are composed of two centrioles, one mature mother centriole with distal and subdistal appendages and one daughter centriole, surrounded by a proteinaceous pericentriolar material (PCM) (Conduit *et al*, 2015). During mitosis, centrosomes help assemble the mitotic spindle, and during interphase, the mother centriole forms the basal body template for cilia (Bornens, 2012). In proliferating cells, centrioles can form *de novo* without pre-existing centrioles or use the scaffold of existing centrioles to duplicate once per cell cycle in late G1 and S phases (Loncarek & Khodjakov, 2009). The centriole formation pathway has been defined in cell culture and in different organisms and relies on a set of core proteins that include spindle assembly defective protein 4 (SAS-4, also called CENPJ or CPAP; Kirkham *et al*, 2003; Leidel & Gonczy, 2003; Kleylein-Sohn *et al*, 2007; Tang *et al*, 2009). The newly formed centrioles undergo maturation over two cell cycles to acquire appendages, such as ODF2 and CEP164, become MTOCs and template cilia (Kong *et al*, 2014). Cilia formation relies on docking of the mother centriole to the plasma membrane through distal appendage proteins, such as CEP164 (Graser *et al*, 2007; Siller *et al*, 2017), and on intra-flagellar transport proteins, such as IFT88 (Haycraft *et al*, 2007).

During rodent development, and unlike the development of most organisms, the first cell divisions post-fertilization occur without centrioles (Woolley & Fawcett, 1973; Gueth-Hallonet *et al*, 1993; Manandhar *et al*, 1998; Courtois *et al*, 2012; Howe & FitzHarris, 2013). In the mouse embryo, centrioles first form by *de novo* biogenesis starting at the blastocyst stage around embryonic day (E) 3.5 (Courtois & Hiiragi, 2012). Before centriole formation, diffuse γ-tubulin signals, a PCM component and microtubule nucleator, appear at the morula stage around E3, and γ-tubulin signals become more focused as centrioles form; however, the newly formed centrioles do not seem to act as MTOCs in interphase cells (Howe & FitzHarris, 2013). In addition, the first cilia form almost two days post-implantation around E6.5 in cells of the epiblast (Bangs *et al*, 2015).

Mouse embryonic stem cells (mESCs) are a well-established *in vitro* model of embryo development that are derived from the

1 Department of Dermatology and Venereology, University Hospital of Cologne, Cologne, Germany
2 The Cologne Cluster of Excellence in Cellular Stress Responses in Aging-associated Diseases (CECAD), University of Cologne, Cologne, Germany
3 Graduate Program in Pharmacology and Experimental Therapeutics, University Hospital of Cologne, Cologne, Germany
4 Graduate School for Biological Sciences, University of Cologne, Cologne, Germany
5 Masters Program in Biological Sciences, University of Cologne, Cologne, Germany
*Corresponding author. Tel: +49 221 478 84385; E-mail: hisham.bazzi@uk-koeln.de
†These authors contributed equally to this work
‡Present address: Laboratory of Neuro Imaging, USC Stevens Neuroimaging and Informatics Institute, Keck School of Medicine of University of Southern California, Los Angeles, CA, USA

pluripotent inner cell mass of blastocysts at E3.5 but molecularly resemble epiblast cells post-implantation (Nichols & Smith, 2011). To maintain uniform pluripotency, mESCs are cultured with leukemia inhibitory factor (LIF) and two other differentiation inhibitors abbreviated as 2i (Williams *et al*, 1988; Ying *et al*, 2008). In pluripotency, the transcription factor NANOG is highly expressed in mESCs and regulates self-renewal (Rosner *et al*, 1990). In this study, we used mESCs to complement our *in vivo* experiments by studying the growth dynamics of cells without centrioles.

We have previously shown that the genetic removal of SAS-4 in the mouse resulted in the loss of centrioles and cilia (Bazzi & Anderson, 2014a). The $Sas\text{-}4^{-/-}$ embryos arrested development around E9.5 due to p53-dependent cell death. The increase in p53 in $Sas\text{-}4^{-/-}$ embryos was not due the secondary loss of cilia, DNA damage or chromosome segregation errors. Also, these phenotypes are not specific to $Sas\text{-}4^{-/-}$ embryos because mutations in different genes, such as *Cep152*, that cause centriole loss show similar phenotypes (Bazzi & Anderson, 2014a, b). Notably, the fraction of mitotic cells was higher in $Sas\text{-}4^{-/-}$ embryos at E7.5 and E8.5, indicating a longer mitotic duration of cells without centrioles, which was also confirmed by time-lapse imaging of dividing cells. Because a short nocodazole treatment to prolong mitosis upregulated p53 in cultured wild-type (WT) embryos, the data suggested that the less efficient mitosis without centrioles activated a novel p53-dependent pathway (Bazzi & Anderson, 2014a). In cultured mammalian cell lines *in vitro*, a similar pathway that is activated by the loss of centrioles or prolonging mitosis leads to p53-dependent cell cycle arrest and has been termed the mitotic surveillance pathway (Lambrus *et al*, 2015; Wong *et al*, 2015; Lambrus & Holland, 2017). Recently, p53-binding protein 1 (53BP1) and ubiquitin specific peptidase 28 (USP28) have been shown to be essential for the conduction of this pathway *in vitro* (Fong *et al*, 2016; Lambrus *et al*, 2016; Meitinger *et al*, 2016). These studies showed that mutations in *53BP1* or *USP28* rescued the growth arrest phenotype observed in cells without centrioles. However, whether a similar 53BP1- and USP28-dependent pathway operates *in vivo* and can cause the p53-dependent cell death phenotype in the mouse are still not known.

In this study, our data showed that the mitotic surveillance pathway is conserved in mice *in vivo* and that 53BP1 and USP28 are essential for its conduction upstream of p53. In order to explain the late onset of the phenotype upon the loss of centrioles, we also asked when during development this pathway is established. The data indicated that the newly formed centrioles around E3 are not fully mature and do not seem to be required for mitosis until around E7 of development, when the pathway is initiated. Our data suggest that once the cells start to depend on centrosomes as MTOCs in mitosis and ciliogenesis, then they sense the loss of centrioles and activate the p53-dependent mitotic surveillance pathway.

Results and Discussion

Mutations in 53bp1 or Usp28 rescue the *Sas-4* mutant phenotype *in vivo*

To test the conservation of the mitotic surveillance pathway and the involvement of 53BP1 and USP28 in its activation *in vivo*, $53bp1^{+/-}$ and $Usp28^{+/-}$ null mouse alleles were generated using CRISPR/Cas9

gene-editing (Fig EV1A and B; see Table 1 in Materials and Methods) and crossed to $Sas\text{-}4^{+/-}$ mice (Bazzi & Anderson, 2014a). Both $Sas\text{-}4^{-/-}53bp1^{-/-}$ and $Sas\text{-}4^{-/-}Usp28^{-/-}$ embryos showed remarkable rescues of the morphology and size compared to the $Sas\text{-}4^{-/-}$ embryos at E9.5 (Fig 1A). $Sas\text{-}4^{-/-}53bp1^{-/-}$ and $Sas\text{-}4^{-/-}Usp28^{-/-}$ embryos both underwent body turning, had visible somites and open heads, and were similar to $Sas\text{-}4^{-/-}p53^{-/-}$ mutants (Bazzi & Anderson, 2014a). At the molecular level, $Sas\text{-}4^{-/-}53bp1^{-/-}$ and $Sas\text{-}4^{-/-}Usp28^{-/-}$ embryos showed highly reduced levels of p53 (Fig 1B and D) and cleaved-Caspase 3 (Cl-CASP3) (Fig 1C and E) and were more similar to controls when compared to $Sas\text{-}4^{-/-}$ embryos (Fig 1B–E). The data indicated that mutating *53bp1* or *Usp28* suppressed both p53 stabilization and p53-dependent cell death upon centriole loss *in vivo* and established the conservation of the mitotic surveillance pathway in the mouse.

The mitotic surveillance pathway is activated around E7

In order to determine when the mitotic surveillance pathway is activated in $Sas\text{-}4^{-/-}$ embryos, we used immunostaining and quantified nuclear p53 levels during development. At E7.5, $Sas\text{-}4^{-/-}$ embryos were smaller than control embryos (WT or $Sas\text{-}4^{+/-}$) with around 1.5-fold higher nuclear p53 in the epiblast (Fig 2A) (Bazzi & Anderson, 2014a). Earlier in development at E6.5, $Sas\text{-}4^{-/-}$ embryos were morphologically indistinguishable from control embryos, and nuclear p53 was not detectably different (Fig 2B). *Ift88* null (cilia mutant) embryos were used as controls for $Sas\text{-}4^{-/-}$ centriole mutant embryos and were similar to WT embryos both morphologically and in terms of p53 nuclear levels at E7.5 (Fig EV2A) and E6.5 (Fig EV2B), confirming our earlier finding that p53 upregulation was due to centriole loss and not the secondary loss of cilia (Bazzi & Anderson, 2014a). The data suggested that the increased level of nuclear p53 in $Sas\text{-}4^{-/-}$ embryos starts around E7 of development and is independent of cilia loss *per se*.

USP28 and 53BP1 are expressed in the epiblast before E6

We next asked whether the upregulation of p53 in $Sas\text{-}4^{-/-}$ embryos around E7, and not before, coincided with the onset of expression of either 53BP1 or USP28, the upstream regulators of p53, in developing WT embryos. We performed immunostaining of 53BP1 and USP28 in WT embryos at E6.5 (Fig 2C) and E5.5 (Fig 2D) and found that both 53BP1 and USP28 were highly expressed in the epiblast of WT embryos at both stages. Of note, both proteins were clearly detectable in the embryonic epiblast but had much lower levels in the surrounding visceral endoderm (Fig 2C and D). The data indicated that the regulation of the onset of 53BP1 or USP28 expression does not seem to be responsible for p53 upregulation and activation of the mitotic surveillance pathway in $Sas\text{-}4^{-/-}$ embryos, suggesting that other mechanisms establish the pathway around E7.

The proper growth of $Sas\text{-}4^{-/-}$ mESCs is dependent on p53

To study the dynamics of the mitotic surveillance pathway activation, we derived primary mESCs from WT and $Sas\text{-}4^{-/-}$ blastocysts at E3.5. $Sas\text{-}4^{-/-}$ primary mESCs were successfully derived and propagated *in vitro* and lacked detectable centrosomes in interphase cells, as judged by γ-tubulin (TUBG) staining, compared to WT
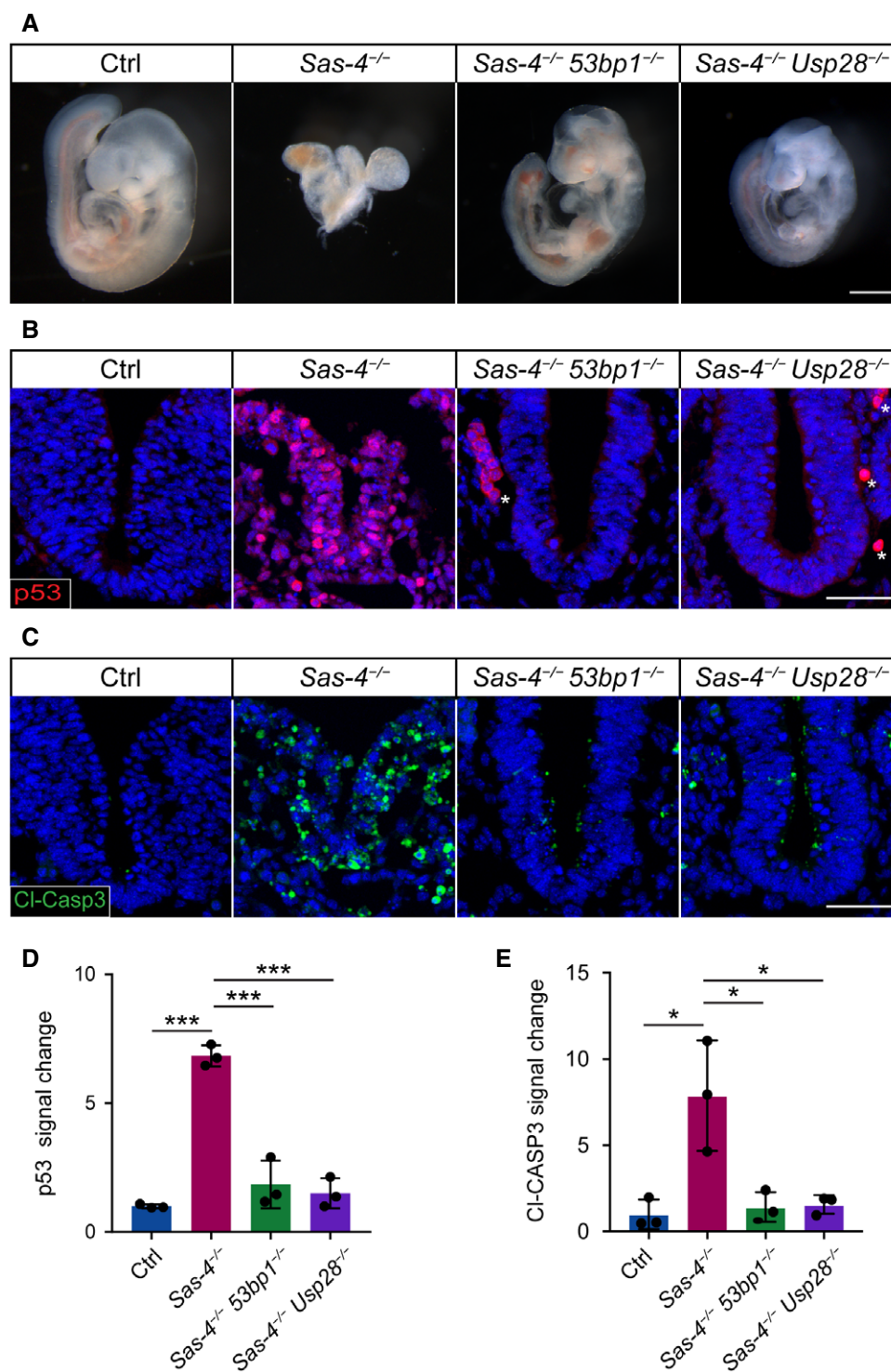
A

B

C

D

E

Figure 1.   The mitotic surveillance pathway is conserved in the mouse *in vivo*.

A   Gross morphology of control (Ctrl), *Sas-4$^{-/-}$*, *Sas-4$^{-/-}$53bp1$^{-/-}$*, and *Sas-4$^{-/-}$Usp28$^{-/-}$* embryos at E9.5. At least five embryos were considered per genotype and all the double mutant embryos exhibited the rescue criteria mentioned in the text. Scale bar = 500 μm.

B, C   Immunostaining for p53 (B) and Cleaved-Caspase3 (Cl-CASP3, (C)) on transverse sections of Ctrl, *Sas-4$^{-/-}$*, *Sas-4$^{-/-}$53bp1$^{-/-}$*, and *Sas-4$^{-/-}$Usp28$^{-/-}$* embryos at E9.5. The area shown encompasses the ventral neural tube and surrounding mesenchyme. Asterisks in (B) denote non-specific staining of blood cells. Scale bar = 50 μm.

D, E   Quantifications of the p53 (D) and Cl-CASP3 (E) fluorescence signals shown in (B) and (C), respectively. Three embryos per genotype were used for the quantifications. ***$P < 0.001$, *$P < 0.05$ (two-tailed Student's *t*-test, one-way ANOVA with Tukey's multiple comparisons tests gave similar results). Bars represent mean ± s.d. (D) Ctrl: 1.00 ± 0.06 ($n = 1,770$ cells); *Sas-4$^{-/-}$*: 6.84 ± 0.34 ($n = 275$), *Sas-4$^{-/-}$53bp1$^{-/-}$*: 1.85 ± 0.75 ($n = 690$), *Sas-4$^{-/-}$Usp28$^{-/-}$*: 1.50 ± 0.48 ($n = 975$). (E) Ctrl: 1.00 ± 0.70 ($n = 1,690$); *Sas-4$^{-/-}$*: 7.88 ± 2.62 ($n = 175$); *Sas-4$^{-/-}$53bp1$^{-/-}$*: 1.43 ± 0.71 ($n = 1030$); *Sas-4$^{-/-}$Usp28$^{-/-}$*: 1.57 ± 0.44 ($n = 950$).
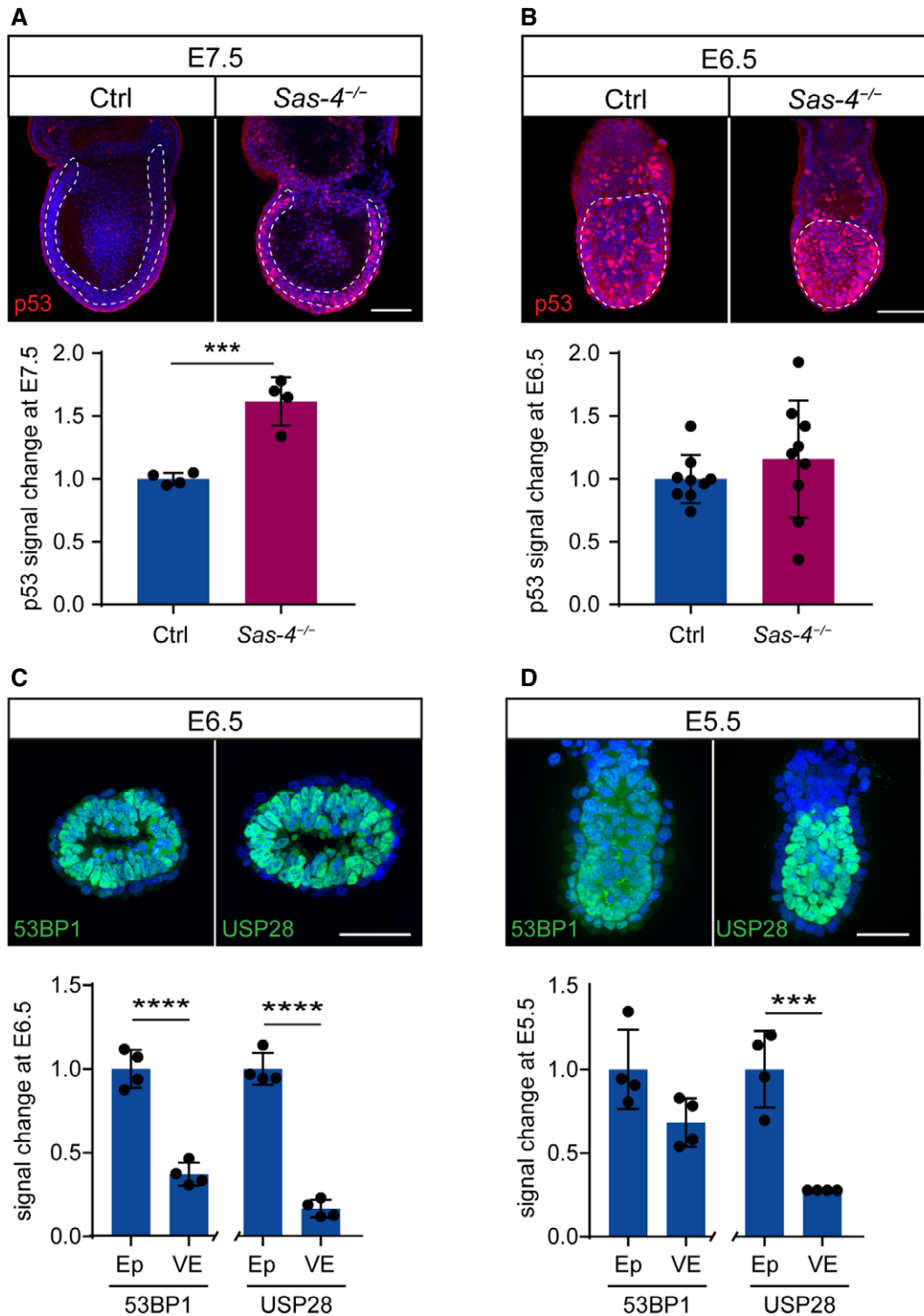
Figure 2. p53 upregulation in *Sas-4*$^{-/-}$ embryos is evident by E7.5 and is not due to the onset of 53BP1 or USP28 expression.

A, B Whole-mount immunostaining and quantification for p53 on Ctrl and *Sas-4*$^{-/-}$ embryos at E7.5 (A) and E6.5 (B). Representative sagittal planes are shown and the dotted lines demarcate the epiblast. Quantification of nuclear p53 fluorescence intensity in the epiblast is shown below, normalized to control embryos in the same batch at E7.5 (4 embryos) and at E6.5 (9 embryos). ***$P < 0.001$ (two-tailed Student's *t*-test). Bars represent mean $\pm$ s.d. Scale bars = 100 μm. (A) Ctrl: 1.04 $\pm$ 0.00 ($n = 495$ cells); *Sas-4*$^{-/-}$: 1.65 $\pm$ 0.19 ($n = 850$). (B) Ctrl: 1.00 $\pm$ 0.18 ($n = 1,665$); *Sas-4*$^{-/-}$: 1.16 $\pm$ 0.44 ($n = 1,330$).

C, D Immunostaining for 53BP1 and USP28 on sagittal sections of WT embryos at E6.5 (C) or sagittal planes of whole-mount immunostaining at E5.5 (D). Quantification of the fluorescent signals in the epiblast (Ep) versus visceral endoderm (VE) are shown below. Four embryos per genotype were used for the quantifications. ****$P < 0.0001$, ***$P < 0.001$ (two-tailed Student's *t*-test). Bars represent mean $\pm$ s.d. Scale bar = 50 μm. (C) 53BP1 in Ep: 1.00 $\pm$ 0.10 ($n = 225$ cells); 53BP1 in VE: 0.37 $\pm$ 0.06 ($n = 105$); USP28 in Ep: 1.00 $\pm$ 0.08 ($n = 235$); USP28 in VE: 0.17 $\pm$ 0.05 ($n = 90$). (D) 53BP1 in Ep: 1.00 $\pm$ 0.24 ($n = 225$); 53BP1 in VE: 0.68 $\pm$ 0.14 ($n = 115$); USP28 in Ep: 1.00 $\pm$ 0.23 ($n = 280$); USP28 in VE: 0.28 $\pm$ 0.00 ($n = 110$).
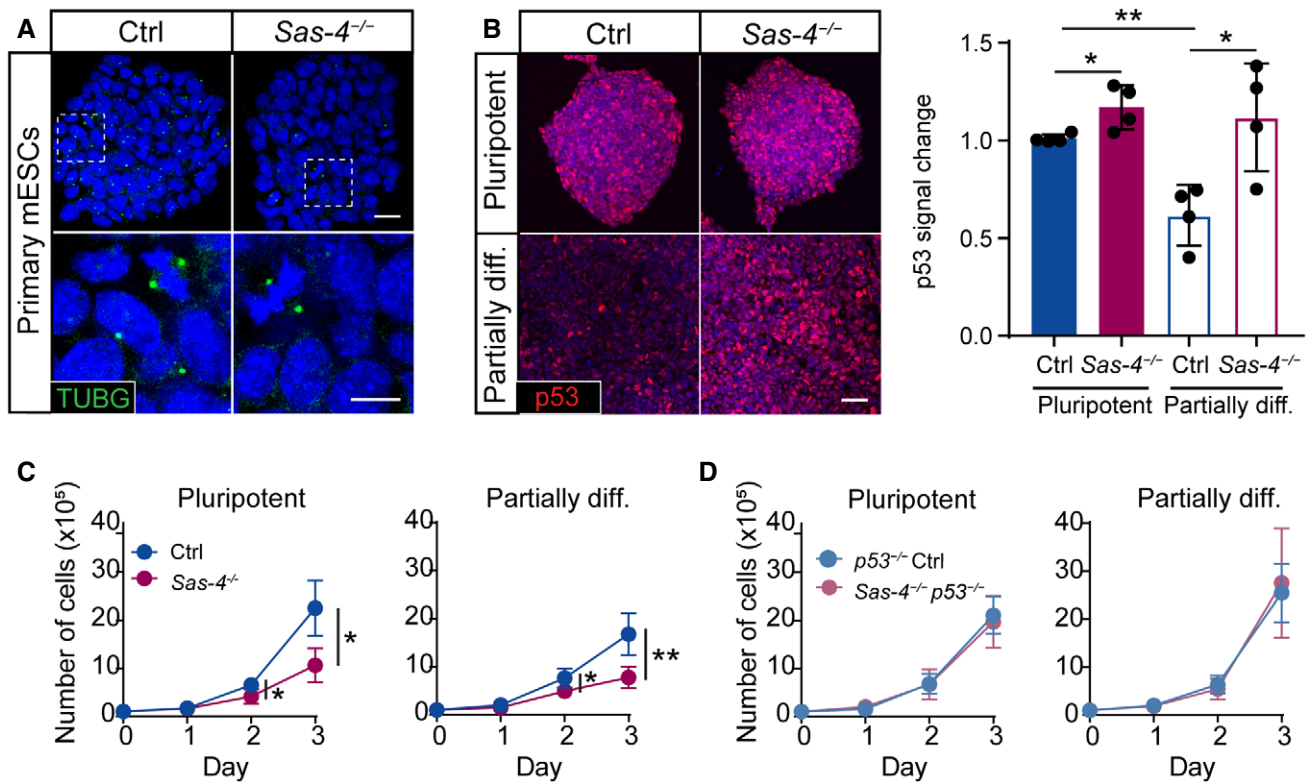
Figure 3. *Sas-4$^{-/-}$* mESCs activate the mitotic surveillance pathway.

A   Immunostaining for the centrosome marker γ-tubulin (TUBG) on Ctrl and *Sas-4$^{-/-}$* primary mESCs. The bottom panels are magnifications of the areas marked in the top panels. Scale bars = 20 μm (top) and 10 μm (bottom).

B   Immunostaining and quantification for p53 on Ctrl and *Sas-4$^{-/-}$* primary mESCs in pluripotent and partially differentiated (diff.) conditions. The quantification of p53 fluorescence intensities was normalized to Ctrl (Four independent experiments). **$P < 0.01$, *$P < 0.05$ (two-tailed Student's *t*-test, the comparison of the genotypes in the "Pluripotent" condition was not significant using the one-way ANOVA with Tukey's multiple comparisons tests). Bars represent mean ± s.d. Scale bar = 50 μm. Pluripotent Ctrl: 1.00 ± 0.02 (n = 2,030 cells); pluripotent *Sas-4$^{-/-}$*: 1.17 ± 0.10 (n = 2,170); partially diff. Ctrl: 0.62 ± 0.13 (n = 2,745); partially diff. *Sas-4$^{-/-}$*: 1.12 ± 0.24 (n = 2,000).

C, D Three-day growth curves of WT and *Sas-4$^{-/-}$* (C) or *p53$^{-/-}$* and *Sas-4$^{-/-}$p53$^{-/-}$* (D) primary mESCs in the indicated conditions starting with 10^5 cells on Day 0 (Four independent experiments). **$P < 0.01$, *$P < 0.05$ (two-tailed Student's *t*-test). Bars represent mean ± s.d. For details of the measurements, see Materials and Methods (Tables 3 and 4).

cells, which had centrosomes in every cell (Fig 3A). TUBG aggregates were seen only at the poles of mitotic cells in *Sas-4$^{-/-}$* mESCs, consistent with our findings in *Sas-4$^{-/-}$* embryos where these PCM aggregates lacked centrioles (Bazzi & Anderson, 2014a). Both WT and *Sas-4$^{-/-}$* primary mESCs showed high levels of nuclear NANOG in media containing LIF and 2i, indicating their pluripotent potential (Fig EV3A). In pluripotent conditions (LIF and 2i), WT and *Sas-4$^{-/-}$* primary mESCs had seemingly similar levels of p53, as judged by immunostaining (Fig 3B). Because *Sas-4$^{-/-}$* embryos upregulated p53 starting after E6.5 (Fig 2A and B), we reasoned that *Sas-4$^{-/-}$* mESC partial differentiation may trigger a similar response *in vitro*. Thus, we removed the pluripotency factors (LIF and 2i) for three days, and the pluripotency potential declined as shown by the decrease in NANOG nuclear signal in both WT and *Sas-4$^{-/-}$* mESCs (Fig EV3A). The partially differentiated mESCs are not likely to represent a specific lineage because mESCs first move into a transitional state as they exit self-renewal (Martello & Smith, 2014). Importantly, upon partial differentiation, nuclear p53 levels decreased in WT but not in *Sas-4$^{-/-}$* mESCs (Fig 3B). Quantification of the normalized nuclear p53 levels revealed that they were

slightly, but significantly, higher in *Sas-4$^{-/-}$* mESCs compared to WT mESCs in pluripotent conditions, and this difference appeared more pronounced upon partial differentiation (Fig 3B). Also, the decrease in p53 in WT mESCs upon partial differentiation was significant (Fig 3B).

Although *Sas-4$^{-/-}$* mESCs could be derived and propagated in pluripotent condition cultures, we noticed that they grew slower than WT mESCs (Fig 3C). The growth defect became more obvious upon partial differentiation (Fig 3C). To check whether the slower growth in *Sas-4$^{-/-}$* mESCs was dependent on p53 and the possible activation of the mitotic surveillance pathway, we generated *Sas-4$^{-/-}$p53$^{-/-}$* and *p53$^{-/-}$* control mESCs using CRISPR/Cas9 (Fig EV3B, see Table 2 in Materials and Methods). The data showed that *Sas-4$^{-/-}$p53$^{-/-}$* completely rescued the growth delay phenotype relative to *p53$^{-/-}$* and WT mESCs under pluripotent and partially differentiated conditions (Fig 3D). The pathways and molecular players operating upstream as well as downstream of p53 that lead to the growth defect in *Sas-4$^{-/-}$* mESCs, and whether they involve cell cycle regulation or cell death, are currently not known.
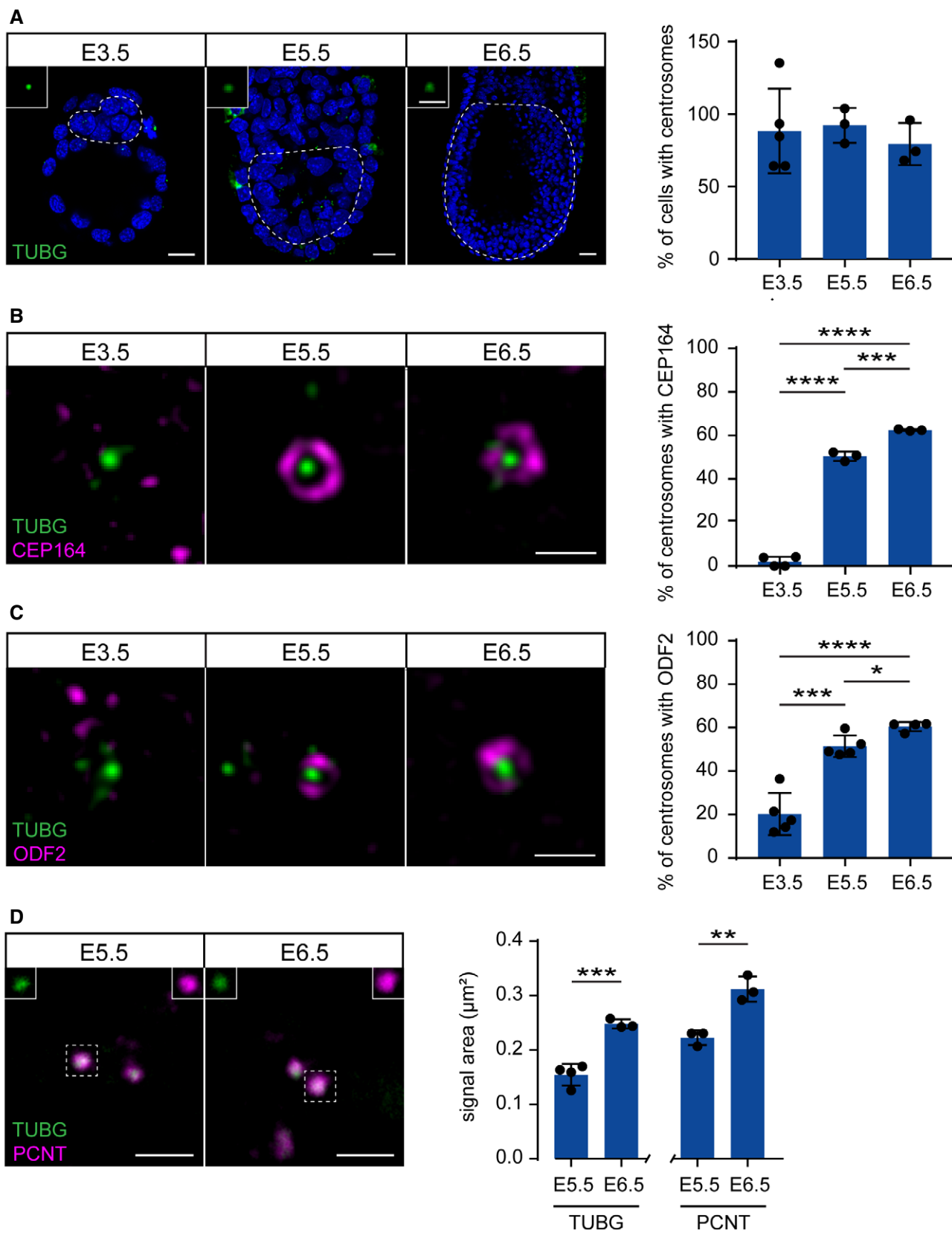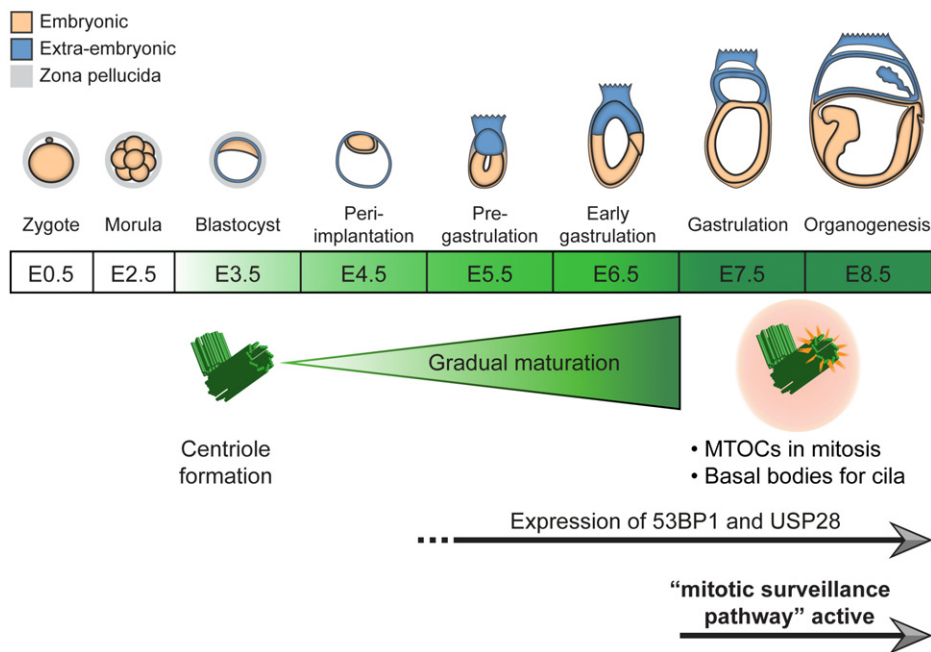
Figure 4.

Figure 4. Centrioles gradually mature during mouse development.

A   Sagittal planes of whole-mount immunostaining and quantification for TUBG on WT mouse embryos from E3.5 to E6.5. The insets are magnifications of selected centrosomes from the dotted areas denoting the inner cell mass (E3.5) or epiblast (E5.5 and E6.5). Bars represent mean ± s.d (two-tailed Student's *t*-test or one-way ANOVA with Tukey's multiple comparisons tests). Scale bars: E3.5 and E5.5 = 15 μm; E6.5 = 30 μm and 3 μm (insets). E3.5: $88 \pm 26\%$ ($n = 73$ cells from 5 embryos); E5.5: $92 \pm 10\%$ ($n = 270$ from 3 embryos); E6.5: $79 \pm 12\%$ ($n = 12{,}082$ from 3 embryos).

B, C   Representative gSTED super-resolution images of immunostaining for TUBG and either CEP164 (B) or ODF2 (C). Whole-mount staining was used for the CEP164 data as well as for the E3.5 blastocysts for ODF2, whereas staining on sections was used for ODF2 at E5.5 and E6.5. Quantification of the percentage of centrosomes (TUBG) with CEP164 or ODF2 are shown on the right. $****P < 0.0001$, $***P < 0.001$, $*P < 0.05$ (two-tailed Student's *t*-test or one-way ANOVA with Tukey's multiple comparisons tests; the ODF2 data between E5.5 and E6.5 was not significant using the latter test). Bars represent mean ± s.d. Scale bar = 0.5 μm. CEP164 at E3.5: $2 \pm 2\%$, ($n = 92$ centrosomes from 4 embryos); E5.5: $50 \pm 2\%$ ($n = 249$ from 3 embryos); E6.5: $62 \pm 0\%$ ($n = 856$ from 3 embryos). ODF2 at E3.5: $20 \pm 9\%$ ($n = 108$ from 5 embryos); E5.5: $51 \pm 4\%$ ($n = 294$ from 5 embryos); E6.5: $60 \pm 2\%$ ($n = 1{,}183$ from 3 embryos).

D   Immunostaining and quantification of the area of TUBG and PCNT signals from E5.5 and E6.5 centrosomes in epiblast cells. The separate channels for the marked centriole are shown in the insets. $***P < 0.001$, $**P < 0.01$ (two-tailed Student's *t*-test). Bars represent mean ± s.d. Scale bar = 2 μm. Quantification of PCNT at E5.5: 0.22 ± 0.01 μm ($n = 103$ centrosomes from 3 embryos); E6.5: 0.31 ± 0.02 μm ($n = 342$ from 3 embryos). Quantification of TUBG at E5.5: 0.15 ± 0.02 μm ($n = 108$ from 4 embryos); E6.5: 0.25 ± 0.01 μm ($n = 311$ from 3 embryos).

Figure 5. A schematic model depicting the correlation between gradual centriole maturation and centrosome functions during mouse embryonic development.

Centrioles first form by *de novo* biogenesis around E3 and gradually mature, acquire appendages (orange spokes) and recruit PCM (pink circle) to provide a basal body template for cilia and act as MTOCs for mitosis around E7, when the mitotic surveillance pathway is established. The expression of 53BP1 and USP28 precedes the establishment of the pathway and continues until at least E9.5. The embryo development timeline was adapted and modified from (Kojima *et al*, 2014).

Mitotic surveillance pathway activation is associated with prolonged mitosis *in vivo* and *in vitro*

We have previously shown that prometaphase was prolonged in *Sas-4*$^{-/-}$ embryos at E7.5 and at E8.5 (Bazzi & Anderson, 2014a). To address whether the activation of the mitotic surveillance pathway around E7 coincided with the onset of prolonged mitosis in *Sas-4*$^{-/-}$ embryos, we performed immunostaining for the mitotic marker phospho-histone H3 (pHH3) at E6.5. We calculated the mitotic index, the percentage of pHH3-positive cells in the epiblast, as an indirect measure of mitotic duration and detected no

difference between control and *Sas-4*$^{-/-}$ embryos at E6.5 (Fig EV3C). In contrast, our previous data showed that the mitotic index of *Sas-4*$^{-/-}$ embryos at E7.5 was significantly higher than that of control embryos (Fig EV3D) (Bazzi & Anderson, 2014a). The data indicated that the mitotic surveillance pathway activation through p53 upregulation temporally correlates with prolonged mitosis *in vivo*.

In line with the embryo data *in vivo*, the mitotic indices of WT and *Sas-4*$^{-/-}$ mESCs *in vitro* were similar in pluripotency. In contrast, upon partial differentiation, the mitotic index of *Sas-4*$^{-/-}$ mESCs was significantly higher than that of WT mESCs (Fig EV3E).

These findings suggested that the potential enhanced activation of the mitotic surveillance pathway in mESCs also correlates with prolonged mitosis upon partial differentiation, and that the growth dynamics of $Sas\text{-}4^{-/-}$ mESCs largely resemble those of $Sas\text{-}4^{-/-}$ embryos. However, ~4% of WT mESCs were ciliated in pluripotency and the percentage doubled to ~8%, but was not significant, upon partial differentiation (Fig EV3F). Lineage-directed differentiation methods of mESCs maybe required to uncover the full spectrum of defects in $Sas\text{-}4^{-/-}$ mESCs and assess whether they are dependent on p53 and/or cilia formation.

Gradual centriole maturation correlates with the establishment of the mitotic surveillance pathway *in vivo*

We next hypothesized that the centrioles that are first formed by *de novo* biogenesis around E3 were not fully mature yet and that their maturation correlates with the delayed response to centriole loss in $Sas\text{-}4^{-/-}$ embryos around E7. Therefore, we performed immunostaining, also combined with super-resolution imaging, for TUBG together with either the distal appendage protein CEP164 or the subdistal appendage ODF2, both representing appendage markers of the more mature mother centrioles, on developing embryos between E3.5 and E6.5 (Fig 4A–C). Starting at E3.5, almost all the cells contained centrosomes marked by TUBG foci (Fig 4A). Intriguingly, neither CEP164 (Fig 4B) nor ODF2 (Fig 4C) localized to these centrosomes at E3.5, supporting our hypothesis that the centrioles were not mature. At E5.5, around 50% of the centrosomes in the epiblast colocalized with CEP164 or ODF2, and the percentage increased to around 60% at E6.5 (Fig 4B and C). In addition, the ability to recruit more PCM is another measure of centriole maturation; therefore, we quantified the areas of immunostaining signals for two PCM proteins, TUBG and PCNT, in developing WT embryos (Fig 4D). The data showed that the centrosomes of epiblast cells at E6.5 recruited significantly more TUBG and PCNT compared to those at E5.5 (Fig 4D). We concluded that the newly formed centrioles in mouse embryos gradually mature, acquire appendages, and recruit more PCM to participate in mitosis and cilia formation around gastrulation overlapping with the activation of the mitotic surveillance pathway in $Sas\text{-}4^{-/-}$ centriole mutant embryos around E7 (Fig 5). A causal relationship between centriole maturation and pathway activation is still elusive.

Although mitosis is usually the shortest phase of the cell cycle and lasts only around half an hour, it is an essential phase where the segregation of DNA and other cellular components must be precisely accomplished. In addition to the well-studied spindle assembly checkpoint (SAC), mammalian cells have developed a newly discovered pathway to monitor mitosis termed the mitotic surveillance pathway that is independent of the SAC (Lambrus & Holland, 2017). This pathway seems to be limited to mammalian systems because organisms such as *Drosophila melanogaster* lack 53PB1 and USP28 homologs (Lambrus & Holland, 2017), and zygotic *Sas-4* mutant flies survive until adulthood (Basto *et al*, 2006).

Both control and $Sas\text{-}4^{-/-}$ embryos show relatively high nuclear p53 around E6.5, which has been reported in WT embryos at E5.5 and E6.5 (Bowling *et al*, 2018). It has been suggested that p53 may be involved in cellular competition during this stage of development to eliminate less fit cells before the

germline is selected (Zhang *et al*, 2017). Higher p53 levels in $Sas\text{-}4^{-/-}$ embryos around E7 coincide with the window of the initiation of gastrulation as well as the appearance of cilia on epiblast-derived lineages (Bangs *et al*, 2015). Our data largely exclude the lack of cilia *per se* (Fig EV2) or the expression of the mitotic surveillance pathway components (Fig 2C and D) as determinants of pathway activation after a lag period and at a specific developmental window. In line with this, 53BP1 expression has been reported throughout mouse pre-implantation development (Ziegler-Birling *et al*, 2009). In addition, the expression of 53BP1 and USP28 was mostly restricted to the epiblast (Fig 2C and D), which may explain why the fast proliferating epiblast cells seem to be more affected by centriole loss compared to the visceral endoderm (Bazzi & Anderson, 2014a). Collectively, our data support a model whereby the newly formed centrioles around E3 gradually mature during development until around E7, when they are competent to become basal bodies and participate in cilia formation as well as act as efficient MTOCs during mitosis (Fig 5). As such, $Sas\text{-}4^{-/-}$ centriole mutant embryos may not activate the p53-dependent mitotic surveillance pathway until centrioles are more mature and required for mitosis. This gradual transition is reminiscent of the earlier transition from meiotic- to mitotic-like divisions during pre-implantation and may be a general phenomenon in development including, for example, cilia formation, elongation and function (Courtois & Hiiragi, 2012; Bangs *et al*, 2015).

Materials and Methods

Animals and genotyping

The $Sas\text{-}4^{-/-}$ mice ($Cenpj^{tm1d(EUCOMM)Wtsi/tm1d(EUCOMM)Wtsi}$) (Bazzi & Anderson, 2014a) and the $Ift88^{-/-}$ null mouse allele generated from the $Ift88^{fl/fl}$ allele ($Ift88^{tm1Bky}$) (Haycraft *et al*, 2007) were used in this study. The CRISPR/Cas9 endonuclease-mediated knockouts of $53bp1^{-/-}$ and $Usp28^{-/-}$ were generated by the CECAD *in vivo* Research Facility using microinjection or electroporation of the corresponding gRNA, Cas9 mRNA, and Cas9 protein into fertilized zygotes (Table 1) (Chu *et al*, 2016; Troder *et al*, 2018). The gRNA target sequence predictor tool developed by the Broad Institute was used to design gRNAs (Doench *et al*, 2016).

The animals were housed and bred under standard conditions in the CECAD animal facility, and the allele generation (84-02.04.2014.A372) and experiments (84-02.05.50.15.039) were

Table 1. Information for CRISPR/Cas9 and genotyping of *53bp1* and *Usp28* mouse alleles

	53bp1	*Usp28*
Exon	4	2
gRNA	TCTTCTCATTTGGGTACCAG	AATCAGCTGCGAGAAATCAC
Mutation	5 bp deletion and 4 bp insertion (a net of 1 bp deletion)	1 bp insertion
InDel	TCTTCTCATTTG<u>TTCT</u>-CAG	AATCAGCTGCGAGAAA<u>T</u>TCAC
Primer 1	GTGTTTAAGGTCCTGTGGGG	TGATGCTCTGCTCCGAGAAA
Primer 2	AGCTTTAATGTCCCTGCCCA	AAGCCCACTGTACATTCCCA

approved by the Landesamt für Natur, Umwelt, und Verbraucher-schutz Nordrhein-Westfalen (LANUV-NRW) in Germany. All the phenotypes were analyzed in the FVB/NRj background. Genotyping was carried out using standard and published PCR protocols. The PCR products for *53bp1-* and *Usp28*-mutant mice were digested with *Kpn*I and *Apo*I restriction enzymes (New England BioLabs; Ipswich, MA, USA), respectively, to distinguish the WT and mutant alleles.

Wild type (WT) refers to unmodified +/+ alleles and Control (Ctrl) to combinations of +/+ and +/− (heterozygous) alleles for the respective genes.

Mouse embryonic stem cell culture

Primary mESCs were derived from E3.5 blastocysts as previously described (Bryja *et al*, 2006), cultured on feeder cells that were proliferation-inactivated with mitomycin C (Sigma-Aldrich; St. Louis, MO, USA) and 0.1% gelatin-coated plates (Sigma-Aldrich). They were maintained in media containing Knock-Out DMEM (Thermo Fisher Scientific; Waltham, MA, USA), supplemented with 15% HyClone fetal bovine serum (FBS; VWR; Radnor, PA, USA), 2 mM L-glutamine (Biochrom; Berlin, Germany), 1% peni-cillin/streptomycin (Biochrom), 0.1 mM MEM non-essential amino acids (Thermo Fisher Scientific), 1 mM sodium pyruvate (Thermo Fisher Scientific), 0.1 mM β-mercaptoethanol (Thermo Fisher Scientific), 1000 U/ml leukemia inhibitory factor (LIF; Merck; Darmstadt, Germany), and with 1 μM PD0325901 (Miltenyi Biotec; Bergisch Gladbach, Germany) and 3 μM CHIR99021 (Miltenyi Biotec), together abbreviated as 2i. Primary mESCs were gradually weaned off feeder cells and maintained in feeder-free conditions. To induce partial differentiation, feeder-free primary mESCs were split and cultured in media without LIF and 2i for three days.

Generating CRISPR/Cas9-modified primary mESCs

The gRNA sequence for targeting *p53* was cloned as double-stranded DNA oligonucleotides into the *Bbs*I restriction site of the pX330-U6-Chimeric_BB-CBh-hSpCas9 vector (Addgene; Watertown, MA, USA) modified with a Puro-T2K-GFP cassette containing puro-mycin-resistance and eGFP expression by Dr. Leo Kurian's research group (Center for Molecular Medicine Cologne).

Table 2. Information for CRISPR/Cas9-generated *p53* alleles in mESCs

	p53			
Exon	4			
gRNA	AGGAGCTCCTGACACTCGGA			
Cell line	*p53*⁻/⁻		*Sas-4*⁻/⁻*p53*⁻/⁻	
Mutation	16 bp deletion	1 bp deletion	2 bp deletion	1 bp deletion
InDel	TCC------- ---------T	T-CGAGTGTC AGGAGCTCCT	T--GAGTGTC AGGAGCTCCT	TCC-AGTGTC AGGAGCTCCT
Primer 1	TTGTTTTCCAGACTTCCTCCA			
Primer 2	CTGAAGAGGAACCCCCAAAT			

p53⁻/⁻ and *Sas-4*⁻/⁻*p53*⁻/⁻ mESCs (Table 2) were generated by lipofection of the modified pX330 vector containing the gRNA target sequences using Lipofectamine 3000 (Thermo Fisher Scientific). One day after transfection, 2 μg/ml puromycin (Sigma-Aldrich) was added to the medium for two days, and the cells were allowed to recover in regular medium up to one week after transfection. Single colonies were picked under a dissecting microscope and were expanded. *p53* null cell lines were confirmed with sequencing (primers in Table 2), immunofluorescence, and Western blotting.

Growth assay

To determine the growth kinetics of mESCs over three days, WT, *Sas-4*⁻/⁻, *p53*⁻/⁻, and *Sas-4*⁻/⁻*p53*⁻/⁻ mESCs were seeded at 10⁵ cells per well of a 6-well plate in media with or without LIF and 2i in triplicate. One set was counted every day for three days using a hemocytometer. Two pairs of each genotype from separate derivations were counted twice and constituted four biological replicates.

Table 3. The measurements shown in Figure 3C

	Pluripotent [×10⁵ cells]		Partially diff. [×10⁵ cells]	
Day	Ctrl	*Sas-4*⁻/⁻	Ctrl	*Sas-4*⁻/⁻
0	1.00 ± 0.00	1.00 ± 0.00	1.00 ± 0.00	1.00 ± 0.00
1	1.66 ± 0.21	1.59 ± 0.31	2.01 ± 0.45	1.53 ± 0.39
2	6.52 ± 1.01	4.13 ± 1.35	7.65 ± 1.73	4.90 ± 0.84
3	22.53 ± 4.95	10.64 ± 3.07	16.82 ± 3.76	7.80 ± 1.94

Table 4. The measurements shown in Figure 3D

	Pluripotent [×10⁵ cells]		Partially diff. [×10⁵ cells]	
Day	*p53*⁻/⁻_Ctrl	*Sas-4*⁻/⁻*p53*⁻/⁻	*p53*⁻/⁻_Ctrl	*Sas-4*⁻/⁻*p53*⁻/⁻
0	1.00 ± 0.00	1.00 ± 0.00	1.00 ± 0.00	1.00 ± 0.00
1	1.50 ± 0.54	2.00 ± 1.01	2.03 ± 0.54	1.88 ± 0.43
2	6.81 ± 1.82	6.68 ± 2.69	6.39 ± 1.82	5.46 ± 1.87
3	21.09 ± 3.31	19.73 ± 4.67	25.42 ± 3.31	27.52 ± 9.83

Embryo dissection, immunofluorescence and imaging

Pregnant female mice (E3.5 - E9.5) were sacrificed by cervical dislocation for embryo dissections under a dissecting microscope (M165C or M80, Leica Microsystems; Wetzlar, Germany) as previously described (Bryja *et al*, 2006; Behringer *et al*, 2014). The embryos were fixed in 4% paraformaldehyde (PFA; Carl Roth; Karlsruhe, Germany) for 2 h at room temperature or overnight at 4°C. Embryos between E3.5–E6.5 were either fixed in 4% PFA for 30 min and in ice-cold methanol for 15 min, or in pure methanol for 1 h at −20°C for cleaner centrosomal staining. After fixing, the embryos were washed with phosphate-buffered saline (PBS; VWR), and then either used for whole-mount immunostaining or cryoprotected in 30% sucrose overnight at 4°C. The embryos were transferred from 30% sucrose and embedded in optimum cutting

temperature (OCT) compound (Sakura Finetek; Alphen an den Rijn, Netherlands) for cryosectioning.

Whole-mount immunofluorescence staining of intact mouse embryos was performed as previously described (Xiao *et al*, 2018). The embryos were then mounted in 1% low-melting agarose (Lonza; Basel, Switzerland) on a glass bottom dish (Thermo Fisher Scientific), covered in VectaShield mounting medium (Linaris; Dossenheim, Germany) and kept cold and protected from light until imaging. After imaging, the embryos were removed from the agarose, washed, and digested for genotyping. Embryos at E3.5 were either directly imaged in PBS in a glass bottom dish for confocal microscopy or mounted in Prolong Gold (Cell Signaling Technology; Danvers, MA, USA) on a slide for gSTED super-resolution microscopy.

OCT-embedded embryos were cryosectioned at 8 μm thickness and the slides were fixed with ice-cold methanol for 10 min at −20°C, then washed two times with wash buffer containing 0.2% Triton-X in PBS while shaking and blocked with wash buffer with 5% heat-inactivated goat serum for 1 h at room temperature. The slides were incubated with primary antibodies diluted in blocking solution overnight at 4°C. After washing two times with wash buffer, the slides were incubated with secondary antibodies and DAPI in blocking solution for 1 h at room temperature. After washing, the slides were mounted with coverslips using Prolong Gold (Cell Signaling Technology).

For immunostaining of mESCs, 2×10^4 cells were seeded per chamber onto pre-gelatinized Lab-Tek II chamber slides (Thermo Fisher Scientific). After three days of culturing in corresponding media, the cells were washed with PBS, fixed with 4% PFA for 10 min at room temperature and washed three times with PBS. Next, the cells were fixed with ice-cold methanol for 10 min at −20°C, permeabilized with 0.5% Triton-X in PBS for 5 min at room temperature, and blocked with 5% heat-inactivated goat serum (Thermo Fisher Scientific) for at least 15 min at room temperature. The cells were incubated with primary antibodies diluted in blocking solution overnight at 4°C. After washing three times with wash buffer, the cells were incubated with secondary antibodies and DAPI diluted 1:1,000 in blocking solution for 1 h at room temperature. After washing, the chamber was removed from the glass slide and coverslips were mounted using Prolong Gold anti-fade reagent (Cell Signaling Technology). The images were obtained using a TCS gSTED SP8 confocal microscope equipped with gSTED super-resolution (Leica Microsystems). For gSTED imaging, an HC PL APO 93X/1.3 GLYC motCORR objective was used.

Antibodies

Primary antibodies used in this study and their dilutions and sources are listed in Table 5. The secondary antibodies used for confocal microscopy were Alexafluor® 488, 568, or 647 conjugates (Life Technologies) and diluted at 1:1,000, in combination with DAPI (AppliChem) at 1:1,000. For gSTED imaging, the following secondary antibodies and conjugates were used: Abberior® STAR 580 anti-rabbit IgG (Sigma-Aldrich) and FluoTag®-X2 anti-mouse IgG1 coupled to Atto 647N (NanoTag Biotechnologies, Göttingen, Germany).

Image analyses

Images of whole-mount embryos, cryostat sections, or mESCs were quantified using ImageJ (NIH, Maryland, USA). Representative mid-

Table 5. List of primary antibodies used in this study

Antigen	Host	Dilution	Company	Catalog Number
53BP1	Rabbit	1:1,000	Novus Biologicals	NB100-304
CEP164	Rabbit	1:2,000	Proteintech	22227-1-AP
Cl-CASP3	Rabbit	1:400	Cell Signaling	9661
NANOG	Rat	1:200	Affymetrix	14-5761
ODF2	Rabbit	1:500	Proteintech	12058-1-AP
p53	Rabbit	1:500	Leica	P53-CM5P-L
PCNT	Rabbit	1:3,000	BioLegend	923701
pHH3	rabbit	1:400	Merck	06-570
TUBG	mouse IgG1	1:1,000	Sigma-Aldrich	T6557
USP28	rabbit	1:1,000	Sigma-Aldrich	HPA006778

sagittal or cross sections of the embryos, and a maximum projection image of mESCs were used for quantification (Table 5). The DAPI channel was used to set a threshold to obtain a region of interest. For example, p53 and DAPI fluorescence intensities were measured, and the p53 intensity was normalized to the DAPI intensity. The average p53 intensity of controls was set to 1.0, and a fold-change p53 intensity was calculated. Centrosomes (defined as one TUBG focus or two close TUBG foci) and CEP164 or ODF2 foci were manually quantified using ImageJ (NIH). The number of nuclei was quantified using the image-based tool for counting nuclei (ITCN) ImageJ plug-in. For gSTED images, image deconvolution was performed using Huygens Essentials (Scientific Volume Imaging, Hilversum, Netherlands).

Western blotting

mESCs were scraped in radioimmunoprecipitation assay (RIPA) buffer containing 150 mM NaCl, 50 mM Tris pH 7.6, 1% Triton X-100 (Sigma-Aldrich), 0.25% sodium deoxycholate, and 0.1% sodium dodecyl sulfate (SDS; AppliChem; Darmstadt, Germany) with an ethylenediaminetetraacetic acid (EDTA)-free protease inhibitor cocktail (Merck), phosphatase inhibitor cocktail sets II (Merck) and IV (Merck), and phenylmethylsulfonyl fluoride (PMSF; Sigma-Aldrich). Protein concentration was measured with an RC DC protein assay kit (Bio-Rad; Feldkirchen, Germany). 10 μg protein per sample was loaded. SDS-polyacrylamide gel electrophoresis (PAGE) and immunoblotting were performed following standard procedures (Towbin *et al.*, 1979; Kurien & Scofield, 2006). Following SDS–PAGE, the proteins were transferred to polyvinylidene fluoride (PVDF) membranes (Merck) that were activated in methanol (Carl Roth) for 1 min, blocked in 5% milk (Carl Roth) for 1 h, and incubated with an anti-p53 antibody (1:5,000; Leica Biosystems; Buffalo Grove, IL, USA) or an anti-GAPDH antibody (1:10^4; Merck) overnight at 4°C. The membranes were washed with Tris-buffered saline containing Tween 20 (AppliChem; TBST) and incubated with secondary anti-rabbit (GE Healthcare; Chicago, IL, USA) or anti-mouse (GE Healthcare) antibodies linked with horseradish peroxidase (HRP) at 1:10^4 for 1 h at room temperature. Finally, the membranes were washed with TBST and incubated

with enhanced chemiluminescence (ECL; GE Healthcare; Chicago, IL, USA) and signals were detected with on film (GE Healthcare) in a dark room.

Statistical analyses

Statistical analyses comparing two groups or more of data were performed using pair-wise two-tailed Student's *t*-tests or one-way ANOVA with Tukey's multiple comparisons tests which gave consistent and similar results. The statistics with a cutoff for significance of < 0.05 and the graphic representations with standard deviations (s.d.) were all performed using GraphPad Prism 7 (GraphPad Software, San Diego, CA, USA).

Data availability

This study includes no data deposited in external repositories.

Expanded View for this article is available online.

Author contributions

Conceptualization: CX, MG and HB; Methodology: CX, MG, CM-G, MM, RF and HB; Software: CX, MG, CM-G; Formal Analysis: CX, MG, CM-G; Investigation: CX, MG, CM-G, MM, RF and HB; Writing: CX and HB; Visualization: CX, MG, CM-G; Supervision, Project administration and Funding Acquisition: HB.

Conflict of interest

The authors declare that they have no conflict of interest.

References

Bangs FK, Schrode N, Hadjantonakis AK, Anderson KV (2015) Lineage specificity of primary cilia in the mouse embryo. *Nat Cell Biol* 17: 113–122

Basto R, Lau J, Vinogradova T, Gardiol A, Woods CG, Khodjakov A, Raff JW (2006) Flies without centrioles. *Cell* 125: 1375–1386

Bazzi H, Anderson KV (2014a) Acentriolar mitosis activates a p53-dependent apoptosis pathway in the mouse embryo. *Proc Natl Acad Sci USA* 111: E1491–E1500

Bazzi H, Anderson KV (2014b) Centrioles in the mouse: cilia and beyond. *Cell Cycle* 13: 2809

Behringer R, Gertsenstein M, Vintersen Nagy K, Nagy A (2014) *Manipulating the mouse embryo: a laboratory manual*, 4th edn. pp 198–200, 268–271. Cold Spring Harbor, NY: Cold Spring Harbor Laboratory Press

Bornens M (2012) The centrosome in cells and organisms. *Science* 335: 422–426

Bowling S, Di Gregorio A, Sancho M, Pozzi S, Aarts M, Signore M, Schneider MD, Martinez-Barbera JP, Gil J, Rodriguez TA(2018) P53 and mTOR

signalling determine fitness selection through cell competition during early mouse embryonic development. *Nat Commun* 9: 1763

Bryja V, Bonilla S, Arenas E (2006) Derivation of mouse embryonic stem cells. *Nat Protoc* 1: 2082–2087

Chu VT, Weber T, Graf R, Sommermann T, Petsch K, Sack U, Volchkov P, Rajewsky K, Kuhn R (2016) Efficient generation of Rosa26 knock-in mice using CRISPR/Cas9 in C57BL/6 zygotes. *BMC Biotechnol* 16: 4

Conduit PT, Wainman A, Raff JW (2015) Centrosome function and assembly in animal cells. *Nat Rev Mol Cell Biol* 16: 611–624

Courtois A, Hiiragi T (2012) Gradual meiosis-to-mitosis transition in the early mouse embryo. *Results Probl Cell Differ* 55: 107–114

Courtois A, Schuh M, Ellenberg J, Hiiragi T (2012) The transition from meiotic to mitotic spindle assembly is gradual during early mammalian development. *J Cell Biol* 198: 357–370

Doench JG, Fusi N, Sullender M, Hegde M, Vaimberg EW, Donovan KF, Smith I, Tothova Z, Wilen C, Orchard R *et al* (2016) Optimized sgRNA design to maximize activity and minimize off-target effects of CRISPR-Cas9. *Nat Biotechnol* 34: 184–191

Fong CS, Mazo G, Das T, Goodman J, Kim M, O'Rourke BP, Izquierdo D, Tsou MF (2016) 53BP1 and USP28 mediate p53-dependent cell cycle arrest in response to centrosome loss and prolonged mitosis. *Elife* 5: e16270

Graser S, Stierhof YD, Lavoie SB, Gassner OS, Lamla S, Le Clech M, Nigg EA (2007) Cep164, a novel centriole appendage protein required for primary cilium formation. *J Cell Biol* 179: 321–330

Gueth-Hallonet C, Antony C, Aghion J, Santa-Maria A, Lajoie-Mazenc I, Wright M, Maro B (1993) gamma-Tubulin is present in acentriolar MTOCs during early mouse development. *J Cell Sci* 105(Pt 1): 157–166

Haycraft CJ, Zhang Q, Song B, Jackson WS, Detloff PJ, Serra R, Yoder BK (2007) Intraflagellar transport is essential for endochondral bone formation. *Development* 134: 307–316

Howe K, FitzHarris G (2013) A non-canonical mode of microtubule organization operates throughout pre-implantation development in mouse. *Cell Cycle* 12: 1616–1624

Kirkham M, Müller-Reichert T, Oegema K, Grill S, Hyman AA (2003) SAS-4 is a *C. elegans* centriolar protein that controls centrosome size. *Cell* 112: 575–587

Kleylein-Sohn J, Westendorf J, Le Clech M, Habedanck R, Stierhof YD, Nigg EA (2007) Plk4-induced centriole biogenesis in human cells. *Dev Cell* 13: 190–202

Kojima Y, Tam OH, Tam PP (2014) Timing of developmental events in the early mouse embryo. *Semin Cell Dev Biol* 34: 65–75

Kong D, Farmer V, Shukla A, James J, Gruskin R, Kiriyama S, Loncarek J (2014) Centriole maturation requires regulated Plk1 activity during two consecutive cell cycles. *J Cell Biol* 206: 855–865

Kurien BT, Scofield RH (2006) Western blotting. *Methods* 38: 283–293

Lambrus BG, Daggubati V, Uetake Y, Scott PM, Clutario KM, Sluder G, Holland AJ (2016) A USP28-53BP1-p53-p21 signaling axis arrests growth after centrosome loss or prolonged mitosis. *J Cell Biol* 214: 143–153

Lambrus BG, Holland AJ (2017) A New Mode of Mitotic Surveillance. *Trends Cell Biol* 27: 314–321

Lambrus BG, Uetake Y, Clutario KM, Daggubati V, Snyder M, Sluder G, Holland AJ (2015) p53 protects against genome instability following centriole duplication failure. *J Cell Biol* 210: 63–77

Leidel S, Gonczy P (2003) SAS-4 is essential for centrosome duplication in *C. elegans* and is recruited to daughter centrioles once per cell cycle. *Dev Cell* 4: 431–439

Loncarek J, Khodjakov A (2009) Ab ovo or de novo? Mechanisms of centriole duplication. *Mol Cells* 27: 135–142

Manandhar G, Sutovsky P, Joshi HC, Stearns T, Schatten G (1998) Centrosome reduction during mouse spermiogenesis. *Dev Biol* 203: 424−434

Martello G, Smith A (2014) The nature of embryonic stem cells. *Annu Rev Cell Dev Biol* 30: 647−675

Meitinger F, Anzola JV, Kaulich M, Richardson A, Stender JD, Benner C, Glass CK, Dowdy SF, Desai A, Shiau AK *et al* (2016) 53BP1 and USP28 mediate p53 activation and G1 arrest after centrosome loss or extended mitotic duration. *J Cell Biol* 214: 155−166

Nichols J, Smith A (2011) The origin and identity of embryonic stem cells. *Development* 138: 3−8

Rosner MH, Vigano MA, Ozato K, Timmons PM, Poirier F, Rigby PW, Staudt LM (1990) A POU-domain transcription factor in early stem cells and germ cells of the mammalian embryo. *Nature* 345: 686−692

Siller SS, Sharma H, Li S, Yang J, Zhang Y, Holtzman MJ, Winuthayanon W, Colognato H, Holdener BC, Li FQ *et al* (2017) Conditional knockout mice for the distal appendage protein CEP164 reveal its essential roles in airway multiciliated cell differentiation. *PLoS Genet* 13: e1007128

Tang CJ, Fu RH, Wu KS, Hsu WB, Tang TK (2009) CPAP is a cell-cycle regulated protein that controls centriole length. *Nat Cell Biol* 11: 825−831

Towbin H, Staehelin T, Gordon J (1979) Electrophoretic transfer of proteins from polyacrylamide gels to nitrocellulose sheets: procedure and some applications. *Proc Natl Acad Sci USA* 76: 4350−4354

Troder SE, Ebert LK, Butt L, Assenmacher S, Schermer B, Zevnik B (2018) An optimized electroporation approach for efficient CRISPR/Cas9 genome editing in murine zygotes. *PLoS One* 13: e0196891

Williams RL, Hilton DJ, Pease S, Willson TA, Stewart CL, Gearing DP, Wagner EF, Metcalf D, Nicola NA, Gough NM (1988) Myeloid leukaemia inhibitory factor maintains the developmental potential of embryonic stem cells. *Nature* 336: 684−687

Wong YL, Anzola JV, Davis RL, Yoon M, Motamedi A, Kroll A, Seo CP, Hsia JE, Kim SK, Mitchell JW *et al* (2015) Cell biology. Reversible centriole depletion with an inhibitor of Polo-like kinase 4. *Science* 348: 1155−1160

Woolley DM, Fawcett DW (1973) The degeneration and disappearance of the centrioles during the development of the rat spermatozoon. *Anat Rec* 177: 289−301

Xiao C, Nitsche F, Bazzi H (2018) Visualizing the node and notochordal plate in gastrulating mouse embryos using scanning electron microscopy and whole mount immunofluorescence. *J Vis Exp* https://doi.org/10.3791/58321

Ying QL, Wray J, Nichols J, Batlle-Morera L, Doble B, Woodgett J, Cohen P, Smith A (2008) The ground state of embryonic stem cell self-renewal. *Nature* 453: 519−523

Zhang G, Xie Y, Zhou Y, Xiang C, Chen L, Zhang C, Hou X, Chen J, Zong H, Liu G (2017) p53 pathway is involved in cell competition during mouse embryogenesis. *Proc Natl Acad Sci USA* 114: 498−503

Ziegler-Birling C, Helmrich A, Tora L, Torres-Padilla ME (2009) Distribution of p53 binding protein 1 (53BP1) and phosphorylated H2A.X during mouse preimplantation development in the absence of DNA damage. *Int J Dev Biol* 53: 1003−1011